

Essential Ingredient for Radial-Composition Correlations in Two-Component Many-Body Systems: Short-Range Attractive Central Force

Y. Lei (雷杨)^{1,*}

¹ School of Nuclear Science and Technology, Southwest University of Science and Technology, Mianyang 621010, China

(Dated: February 3, 2026)

The linear correlation between RMS radius difference and composition asymmetry in two-component many-body systems is a robust feature observed across nuclear experiments, diverse theoretical models, and metallic nano-alloy cluster calculations. By employing random-interaction ensembles within a Hartree-Fock framework, we demonstrate that this correlation is not a trivial consequence of many-body symmetries. Instead, we identify the short-range, attractive central potential as the essential ingredient for its emergence, a mechanism underpinned by the Moshinsky transformation and the virial theorem within a harmonic-oscillator approximation of such a potential.

The neutron skin thickness, ΔR_{np} —the difference between neutron and proton RMS radii—serves as a vital terrestrial proxy for the equation of state (EOS) of neutron-rich matter [1–7]. It provides a unique laboratory window into the properties of neutron stars, where ΔR_{np} is found to be positively correlated with the symmetry energy slope L [8–10], a parameter that plays a decisive role in characterizing neutron star radii.

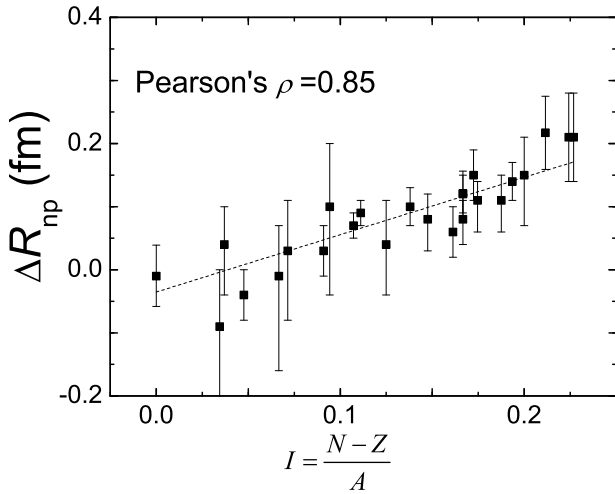


FIG. 1. Experimental ΔR_{np} [11–15] versus isospin asymmetry I . A linear fit indicates a strong correlation with a Pearson coefficient $\rho \approx 0.85$ [16].

A striking feature of ΔR_{np} is its positive linear correlation with the isospin asymmetry $I = (N - Z)/A$, as evidenced by experimental data (Fig. 1). This linear trend is robustly reproduced across diverse theoretical frameworks, e.g., liquid drop models, mean-field theories, and *ab initio* approaches [17–23]. Remarkably, we recently noted that this correlation persists even under random parametrizations of the Skyrme force [24]. The ubiquity of this correlation across various theoretical calculations

suggests that this linearity may be largely independent of specific modeling details, and governed instead by few “ingredients” within the nuclear interaction.

Uncovering these ingredients can be crucial for two reasons. Experimentally, current data is limited to the valley of stability; a fundamental understanding of the $\Delta R_{\text{np}} - I$ correlation allows for more confident extrapolations into the neutron-rich regimes typical of neutron star interiors. Theoretically, identifying these drivers in a shell-model context secures the novel pathway to quantify L via the slope of the $\Delta R_{\text{np}} - I$ correlation proposed previously [24].

In this work, we extract the essential interaction ingredients of the $\Delta R_{\text{np}} - I$ correlation by employing random-interaction ensembles [25–28]. In these ensembles, randomizing interaction matrix elements serves as a statistical “stress test” for the many-body system. Some nuclear properties can survive such a “test”, and thus be identified as robust pattern independent of interaction details, such as the predominance of $I^\pi = 0^+$ ground states [29, 30], the collective-like motions [31–36], odd-even staggering in proton-neutron interactions [37]. Furthermore, specific sampling strategies in random-interaction ensembles allow us to isolate the key interaction components driving these patterns [38–40]. Treating the $\Delta R_{\text{np}} - I$ correlation as such a potential emergent pattern from random-interaction ensembles allows us to pinpoint the essential interaction ingredients governing its existence.

We implement this statistical approach of random interactions within a Hartree-Fock (HF) framework [41–43] across a model space spanning the $0s_{1/2}$ to pf shells. For each random interaction sample, we compute the ground-state RMS radii for both protons and neutrons of nine reference nuclei (^{38}Ar , $^{46,48,50}\text{Ti}$, $^{56,58}\text{Fe}$, $^{60,64}\text{Ni}$, ^{66}Zn) along the stability line with $I \in (0.1, 0.2)$ and evaluate the linearity of the resulting $\Delta R_{\text{np}} - I$ trend using Pearson’s correlation coefficient ρ [16]. An ensemble of 1000 such samples generates a probability distribution of ρ , where a concentration near $\rho \approx 1$ signifies a robust emergence of the correlation.

We begin with the random quasi-particle ensemble

* leiyang19850228@gmail.com

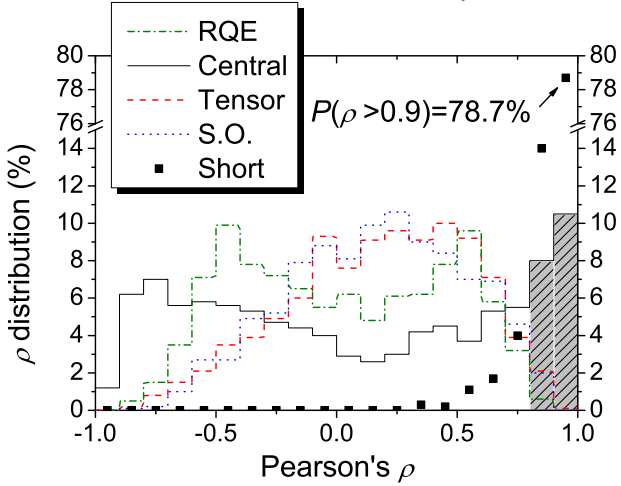


FIG. 2. (Color online) Distributions of Pearson's ρ for the $\Delta R_{np} - I$ correlation across different random ensembles: random quasi-particle (RQE), central, tensor, spin-orbit, and short-range (Short). Radial matrix elements for random central, tensor, and spin-orbit ensembles are randomized via Eq. (1), while the random short-range ensemble employs the radial potential in Eq. (2) with $V_0 = 1$. All distributions are based on 1000 samples from each ensemble with a bin size of 0.1. The shaded region highlights the peak near $\rho = 0.95$ for the random central-force ensemble. Note the broken y -axis; the random short-range ensemble exhibits an exceptionally high rate ($P(\rho > 0.9) \approx 78.7\%$) of strong $\Delta R_{np} - I$ correlation.

(RQE) [29] as a benchmark that maximizes the interaction degrees of freedom while conserving fundamental symmetries, including particle-hole statistical symmetry. As shown in Fig. 2, the RQE yields a negligible probability of strong correlation ($P(\rho > 0.9) < 1\%$), indicating that the $\Delta R_{np} - I$ linearity is not guaranteed by many-body symmetries but requires specific physical ingredients.

To isolate these ingredients, we decompose the nuclear force into its three major components: central, tensor, and spin-orbit forces. These components encompass all interactions that are independent of or linearly dependent on momentum, and compatible with general nuclear symmetries. In our ensemble calculations, their two-body matrix elements are derived from randomized radial matrix element $\langle n'l' | V | nl \rangle$ in the harmonic oscillator (HO) basis via standard reduction formulae [44]. These radial elements are sampled from a Gaussian distribution:

$$\langle n'l' | V | nl \rangle \sim \mathcal{N}(0, \sigma^2 = \frac{1 + \delta_{n'n} \delta_{l'l}}{2}), \quad (1)$$

where the unitary invariance is ensured. As illustrated in Fig. 2, the random tensor and spin-orbit ensembles, like the RQE, fail to produce significant correlations ($P(\rho > 0.9) \approx 0$). In stark contrast, the random central-force ensemble exhibits a pronounced peak at $\rho \approx 0.95$, with nearly 20% of samples displaying strong linearity ($\rho > 0.8$). This statistical filtration unambiguously identifies

the central force as the primary driver of the $\Delta R_{np} - I$ correlation.

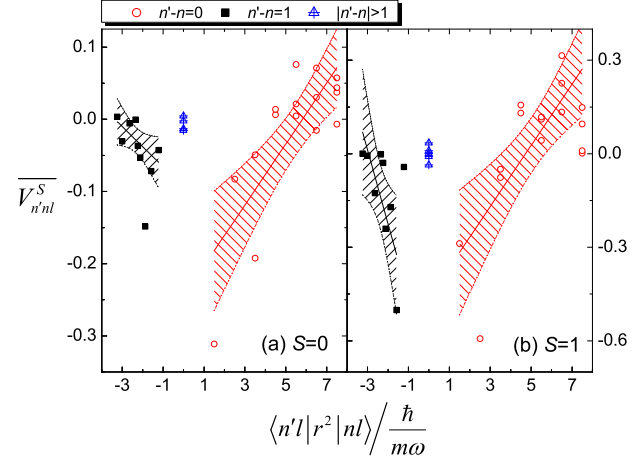


FIG. 3. (Color online) Average of radial matrix elements ($\overline{V_{n'n'l}^S}$) for samples with $\rho > 0.85$ from the random central-force ensemble, plotted against corresponding matrix elements of a 3D harmonic oscillator (HO) potential ($\langle n'l | V(r) = r^2 | nl \rangle$). Symbols distinguish different $n' - n$ selections. The $\overline{V_{n'n'l}^S}$ values exhibit a rough linear scaling with $\langle n'l | r^2 | nl \rangle$ for $n' - n = 0, 1$, while suppress toward 0 for $|n' - n| > 1$, mimicking the HO selection rules.

Despite the central force being the primary driver, not all samples within this ensemble exhibit a strong $\Delta R_{np} - I$ correlation. To identify the specific features that distinguish the "successful" samples ($\rho > 0.85$), we analyze the average of their singlet ($S = 0$) and triplet ($S = 1$) radial matrix elements $\langle n'l | V^S | nl \rangle$, denoted by $\overline{V_{n'n'l}^S}$. Surprisingly, $\overline{V_{n'n'l}^S}$ of these successful samples are roughly correlated with the matrix elements of the HO potential $\langle n'l | r^2 | nl \rangle$. As illustrated in Fig. 3, $\overline{V_{n'n'l}^S}$ effectively "recovers" the HO selection rules: they scale linearly with the HO radial elements for $n' - n = 0, 1$ and suppress toward 0 for $|n' - n| > 1$. This structural fingerprint suggests a possible link between the $\Delta R_{np} - I$ correlation and the HO-like radial potential.

The emergence of the $\Delta R_{np} - I$ correlation from an HO-like potential can be understood as follows. Formally, a system of N nucleons interacting via an HO-type two-body potential can be transformed, via a Moshinsky transformation [45], into a description of independent particles moving in a global HO mean field. In the HO mean field, the energy and mean square radius of HF single-particle states are proportional to each other, according to the virial theorem. Thus, nucleons sequentially occupy levels with increasing energy and, consequently, increasing spatial extent. The accumulation of nucleons thus drives a systematic expansion of the total RMS radius. Therefore, the asymmetry between proton and neutron numbers (I) is inherently correlated to their RMS-radius difference (ΔR_{np}).

To verify this mechanism, we examine the HF single-

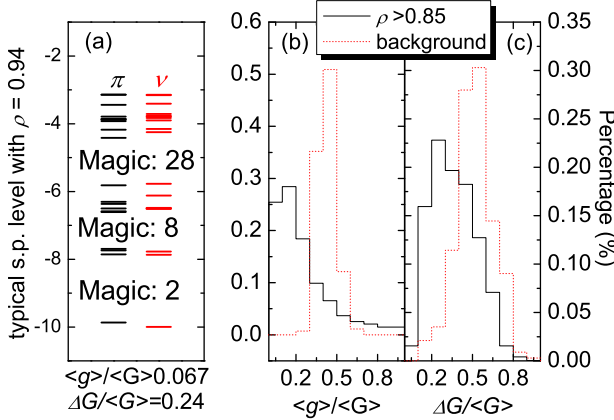


FIG. 4. (Color online) Hartree-Fock (HF) mean-field single-particle properties of samples with the $\Delta R_{\text{np}} - I$ correlation ($\rho > 0.85$) in the random central-force ensemble. (a) Proton and neutron level schemes for a representative sample ($\rho = 0.94$), revealing clear gaps at HO magic numbers (2, 8, 28). (b) Distributions of the gap supremacy $\langle g \rangle / \langle G \rangle$ and (c) the gap equality $\Delta G / \langle G \rangle$. Compared to the stochastic background of randomly distributed levels, samples with $\rho > 0.85$ cluster at lower ratios, signifying characteristics of an HO-like mean field, i.e., the near-degeneracy of intra-shell levels and equal spacing of major gaps.

particle spectra of the successful samples. As shown in Fig. 4(a), these spectra exhibit pronounced shell closures at the HO magic numbers (2, 8, 28). We quantify this "HO-likeness" using two metrics: the ratio of average intra-shell spacing (excluding Kramers degeneracy) to major magic gaps, $\langle g \rangle / \langle G \rangle$, measuring the suppression of intra-shell splitting, and the relative variance of these major gaps, $\Delta G / \langle G \rangle$, measuring the uniformity of major gap spacings. Vanishing values for both metrics would indicate the HO-like intra-shell degeneracy and major-gap uniformity. The distributions in Fig. 4(b) and (c) demonstrate that samples reproducing the $\Delta R_{\text{np}} - I$ correlation are significantly more "HO-like" than the stochastic background of randomly distributed levels, pinpointing an HO-like mean field as the intermediate mechanism for the observed linearity.

To directly examine the influence of the HO potential, we explicitly test a parameterized central HO potential as $V(r) = V_0(r - r_0)^2$. We find that a repulsive HO force ($V_0 < 0$) consistently yields a negative correlation ($\rho \approx -0.8$), contrary to nuclear observations. For attractive forces ($V_0 > 0$), the linearity is remarkably robust against the potential sharpness (V_0), yet sensitive to the potential minimum r_0 . Strong positive correlations ($\rho \approx 1$) only emerge when the minimum is localized within $r_0 < 1.5\sqrt{\hbar/m\omega}$; as r_0 increases, the correlation rapidly degrades to $\rho \approx -0.8$. These results demonstrate that the $\Delta R_{\text{np}} - I$ linearity is a hallmark of an attractive, short-range central HO interaction.

It should be noted that the correlations in Fig. 3 do not imply that the selected samples possess an exact HO po-

tential globally. If that were the case, a rigorous global correlation between $\overline{V_{n'nl}^S}$ and $\langle n'l|r^2|nl \rangle$ would persist across all matrix elements. Instead, $\overline{V_{n'nl}^S}$ represents an ensemble average; individually, a sample may only capture key HO-like features in a few critical two-body elements, which is sufficient to induce the observed $\Delta R_{\text{np}} - I$ linearity. Indeed, any short-range potential with an attractive well near $r = 0$ can be expanded as an HO potential in the low-energy limit. This may explain why the Skyrme force, characterized by a dominant attractive zero-range t_0 term ($t_0 \approx -2.0(5) \times 10^3$ MeV·fm³), frequently reproduces the observed linearity [24], and why diverse theoretical frameworks [20–23] converge on this result by virtue of the short-range attraction inherent in realistic nuclear forces. To confirm this universality, we construct random short-range ensemble with radial potential as

$$V^S(r) \sim \begin{cases} \mathcal{N}(-V_0, 1) & \text{for } r < 1.5\sqrt{\frac{\hbar}{m\omega}}, \\ \mathcal{N}(0, 1) & \text{for } r \geq 1.5\sqrt{\frac{\hbar}{m\omega}} \end{cases}, \quad (2)$$

where a positive V_0 ensures attraction and the critical distance $1.5\sqrt{\hbar/m\omega}$ is informed by our earlier finding regarding the localization of the potential minimum for strong $\Delta R_{\text{np}} - I$ correlation. Remarkably, even with $V_0 = 1$, over 78.7% of the samples exhibit $\rho > 0.9$ (Fig. 2); for $V_0 \geq 2$, the strong linearity becomes an inevitable emergent property, i.e., $P(\rho > 0.9) \approx 100\%$. This ensemble calculations directly identify short-range attraction as the essential ingredient for the $\Delta R_{\text{np}} - I$ correlation.

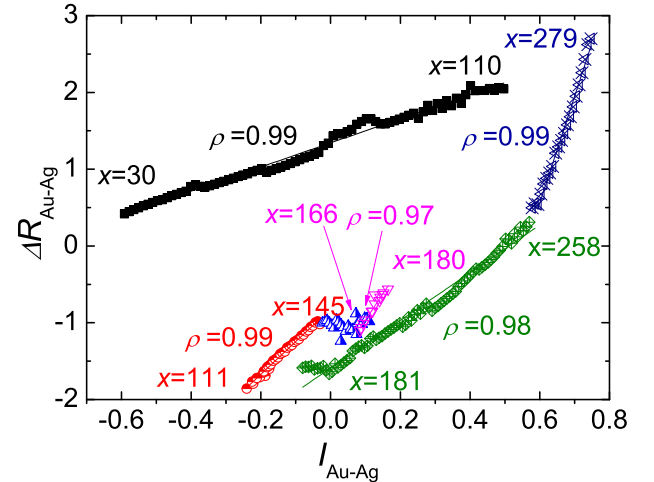


FIG. 5. (Color online) Correlations between the RMS radial difference $\Delta R_{\text{Au-Ag}}$ and atom-number asymmetry $I_{\text{Au-Ag}}$ in the alloy cores of $\text{Au}_x\text{Ag}_{309-x}$ clusters based on many-body calculations from Ref. [46]. Distinct piecewise linearities ($\rho \geq 0.97$) correspond to different shell-filling stages, while the transient region ($x = 145 - 166$) reflects irregular shell occupation in the 2nd shell, as detailed in Ref. [46].

Since our ensemble approach is not restricted to nuclear systems, similar correlation should manifest in any

two-component many-body system governed by short-range attraction. We find a striking confirmation in the structure of $\text{Au}_x\text{Ag}_{309-x}$ nano-alloy clusters [46], where the atom-atom interaction is characterized by a short-range attractive pair potential [47]. To ensure statistical relevance, we focus on clusters with Au and Ag atom numbers no less than 30 ($30 \leq x \leq 279$). By analyzing the authentic alloy core (excluding the surface layer segregated with Ag atoms [48]), and in direct analogy to the nuclear case, we define the RMS radial difference $\Delta R_{\text{Au}-\text{Ag}} = R_{\text{Au}}^{\text{rms}} - R_{\text{Ag}}^{\text{rms}}$ and the atom-number asymmetry $I_{\text{Au}-\text{Ag}} = (N_{\text{Au}} - N_{\text{Ag}})/(N_{\text{Au}} + N_{\text{Ag}})$, where R^{rms} and N denote the root-mean-square radii and atom numbers within the core, respectively. We observe clear correlations between $\Delta R_{\text{Au}-\text{Ag}}$ and $I_{\text{Au}-\text{Ag}}$ in Fig. 5. The observed piecewise linearity directly tracks the evolution of shell occupation already demonstrated in Fig. 2 of Ref. [46]: the segments $x = 30\text{--}110$ and $x = 111\text{--}180$ correspond to the Au-atom filling of the 3rd and 4th shells, respectively, with a chaotic transition at $x = 145\text{--}166$ due to irregular 2nd-shell occupation; subsequent steady growth in both 2nd and 4th shells ($x = 181\text{--}258$) and then stabilized 2nd-shell occupation (up to $x = 279$) yield the remaining linear segments. These distinct segments highlight how the correlation between the RMS radial difference and atom-number asymmetry is sensitive to the specific shell being filled. While nuclear data currently lacks the precision to resolve such shell-breaking effects, the near-perfect linearity of $\Delta R_{\text{Au}-\text{Ag}} - I_{\text{Au}-\text{Ag}}$ correlations in metallic clusters validates our thesis that

short-range attraction is the universal ingredient behind the correlation of the RMS radial difference and composition asymmetry across two-component systems spanning disparate energy and size scales.

In summary, using random-interaction ensembles, we demonstrate that the $\Delta R_{\text{np}} - I$ correlation is not a trivial consequence of many-body symmetries but stems from a key physical ingredient: the short-range attraction of the central nuclear force. As this attraction is a universal feature dominating the nucleon-nucleon interaction, the robust appearance of the $\Delta R_{\text{np}} - I$ linearity across diverse theoretical frameworks [20–24] serves as a structural fingerprint of this fundamental force component. Remarkably, this mechanism is not scale-specific, as evidenced by the similar correlation between RMS radius difference and atom-number asymmetry observed in the alloy core of $\text{Au}_x\text{Ag}_{309-x}$ nano clusters (Fig. 5).

The physical origin of this correlation lies in the geometric properties of the resulting mean field. In the low-energy regime, a short-range attractive potential between nucleons is effectively and approximately mapped onto a global harmonic oscillator (HO) single-particle mean field. Within this framework, the virial theorem for the HO mean field dictates a direct proportionality between a single particle's energy and its mean square radius. Consequently, as nucleons (or atoms) sequentially occupy higher-energy shells, the spatial extent of each species scales with its particle number. This fundamental coupling ensures that any composition asymmetry I is inherently translated into a RMS radius difference ΔR , providing a unified explanation for this linear trend across vastly different many-body systems.

[1] B. Alex Brown, Neutron radii in nuclei and the neutron equation of state, *Phys. Rev. Lett.* **85**, 5296 (2000).

[2] C. J. Horowitz and J. Piekarewicz, Neutron star structure and the neutron radius of ^{208}pb , *Phys. Rev. Lett.* **86**, 5647 (2001).

[3] M. B. Tsang, J. R. Stone, F. Camera, P. Danielewicz, S. Gandolfi, K. Hebeler, C. J. Horowitz, J. Lee, W. G. Lynch, Z. Kohley, R. Lemmon, P. Möller, T. Murakami, S. Riordan, X. Roca-Maza, F. Sammarruca, A. W. Steiner, I. Vidaña, and S. J. Yennello, Constraints on the symmetry energy and neutron skins from experiments and theory, *Phys. Rev. C* **86**, 015803 (2012).

[4] G. Hagen, A. Ekström, C. Forssén, G. R. Jansen, W. Nazarewicz, T. Papenbrock, K. A. Wendt, S. Bacca, N. Barnea, B. Carlsson, C. Drischler, K. Hebeler, M. Hjorth-Jensen, M. Miorelli, G. Orlandini, A. Schwenk, and J. Simonis, Neutron and weak-charge distributions of the ^{48}ca nucleus, *Nature Physics* **12**, 186 (2016).

[5] B. A. Brown, Mirror charge radii and the neutron equation of state, *Phys. Rev. Lett.* **119**, 122502 (2017).

[6] F. J. Fattoyev, J. Piekarewicz, and C. J. Horowitz, Neutron skins and neutron stars in the multimessenger era, *Phys. Rev. Lett.* **120**, 172702 (2018).

[7] C. A. Bertulani and J. Valencia, Neutron skins as laboratory constraints on properties of neutron stars and on what we can learn from heavy ion fragmentation reactions, *Phys. Rev. C* **100**, 015802 (2019).

[8] X. Roca-Maza, M. Centelles, X. Viñas, and M. Warda, Neutron skin of ^{208}Pb , nuclear symmetry energy, and the parity radius experiment, *Phys. Rev. Lett.* **106**, 252501 (2011).

[9] P.-G. Reinhard and W. Nazarewicz, Nuclear charge and neutron radii and nuclear matter: Trend analysis in skyrme density-functional-theory approach, *Phys. Rev. C* **93**, 051303 (2016).

[10] A. Steiner, M. Prakash, J. Lattimer, and P. Ellis, Isospin asymmetry in nuclei and neutron stars, *Physics Reports* **411**, 325 (2005).

[11] J. Zenihiro, H. Sakaguchi, S. Terashima, T. Uesaka, G. Hagen, M. Itoh, T. Murakami, Y. Nakatsugawa, T. Ohnishi, H. Sagawa, H. Takeda, M. Uchida, H. P. Yoshida, S. Yoshida, and M. Yosoi, Direct determination of the neutron skin thicknesses in $^{40,48}\text{ca}$ from proton elastic scattering at $e_p = 295$ mev (2018), [arXiv:1810.11796 \[nucl-ex\]](https://arxiv.org/abs/1810.11796).

[12] J. JASTRZEBSKI, A. TRZCIŃSKA, P. LUBIŃSKI, B. KŁOS, F. J. HARTMANN, T. von EGIDY, and S. WYCECH, Neutron density distributions from an-

tiprotonic atoms compared with hadron scattering data, *International Journal of Modern Physics E* **13**, 343 (2004), <https://doi.org/10.1142/S0218301304002168>.

[13] W. R. Gibbs and J.-P. Dedonder, Neutron radii of the calcium isotopes, *Phys. Rev. C* **46**, 1825 (1992).

[14] D. Adhikari, H. Albataineh, D. Androic, K. A. Aniol, D. S. Armstrong, T. Averett, C. Ayerbe Gayoso, S. K. Barcus, V. Bellini, R. S. Beminiwattha, J. F. Benesch, H. Bhatt, D. Bhatta Pathak, D. Bhetuwal, B. Blaikie, J. Boyd, Q. Campagna, A. Camsonne, G. D. Cates, Y. Chen, C. Clarke, J. C. Cornejo, S. Covrig Dusa, M. M. Dalton, P. Datta, A. Deshpande, D. Dutta, C. Feldman, E. Fuchey, C. Gal, D. Gaskell, T. Gautam, M. Gericke, C. Ghosh, I. Halilovic, J.-O. Hansen, O. Hassan, F. Hauenstein, W. Henry, C. J. Horowitz, C. Jantzi, S. Jian, S. Johnston, D. C. Jones, S. Kakkar, S. Katugampola, C. Keppel, P. M. King, D. E. King, K. S. Kumar, T. Kutz, N. Lashley-Colthirst, G. Leverick, H. Liu, N. Liyanage, J. Mammei, R. Mammei, M. McCaughan, D. McNulty, D. Meekins, C. Metts, R. Michaels, M. Mihovilovic, M. M. Mondal, J. Napolitano, A. Narayan, D. Nikolaev, V. Owen, C. Palatchi, J. Pan, B. Pandey, S. Park, K. D. Paschke, M. Petrusky, M. L. Pitt, S. Premathilake, B. Quinn, R. Radloff, S. Rahman, M. N. H. Rashad, A. Rathnayake, B. T. Reed, P. E. Reimer, R. Richards, S. Riordan, Y. R. Roblin, S. Seeds, A. Shahinyan, P. Souder, M. Thiel, Y. Tian, G. M. Urciuoli, E. W. Wertz, B. Wojtsekhowski, B. Yale, T. Ye, A. Yoon, W. Xiong, A. Zec, W. Zhang, J. Zhang, and X. Zheng (CREX Collaboration), Precision determination of the neutral weak form factor of ^{48}Ca , *Phys. Rev. Lett.* **129**, 042501 (2022).

[15] G. Giacalone, G. Nijs, and W. van der Schee, Determination of the neutron skin of ^{208}Pb from ultrarelativistic nuclear collisions, *Phys. Rev. Lett.* **131**, 202302 (2023).

[16] P. Karl, VII. note on regression and inheritance in the case of two parents, *Proc. R. Soc. Lond.* **58**, 240 (1895).

[17] T. Li, Y. Luo, and N. Wang, Compilation of recent nuclear ground state charge radius measurements and tests for models, *Atomic Data and Nuclear Data Tables* **140**, 101440 (2021).

[18] A. Trzcińska, J. Jastrzębski, P. Lubiński, F. J. Hartmann, R. Schmidt, T. von Egidy, and B. Kłos, Neutron density distributions deduced from antiprotonic atoms, *Phys. Rev. Lett.* **87**, 082501 (2001).

[19] S. J. Novario, D. Lonardoni, S. Gandolfi, and G. Hagen, Trends of neutron skins and radii of mirror nuclei from first principles, *Phys. Rev. Lett.* **130**, 032501 (2023).

[20] W. D. Myers and W. Swiatecki, Average nuclear properties, *Annals of Physics* **55**, 395 (1969).

[21] W. Myers and W. Swiatecki, The nuclear droplet model for arbitrary shapes, *Annals of Physics* **84**, 186 (1974).

[22] W. Myers and W. Swiatecki, Droplet-model theory of the neutron skin, *Nuclear Physics A* **336**, 267 (1980).

[23] C. Pethick and D. Ravenhall, The dependence of neutron skin thickness and surface tension on neutron excess, *Nuclear Physics A* **606**, 173 (1996).

[24] Y. Lei, X. Lian, and C. L. Bai, Robust linear correlations related to neutron skin thickness (2025), *Phys. Rev. C* accepted, 2026, arXiv:2502.05820 [nucl-th].

[25] V. Kota, Embedded random matrix ensembles for complexity and chaos in finite interacting particle systems, *Physics Reports* **347**, 223 (2001).

[26] Y. Zhao, A. Arima, and N. Yoshinaga, Regularities of many-body systems interacting by a two-body random ensemble, *Physics Reports* **400**, 1 (2004).

[27] V. Zelevinsky and A. Volya, Nuclear structure, random interactions and mesoscopic physics, *Physics Reports* **391**, 311 (2004), from atoms to nuclei to quarks and gluons: the omnipresent manybody theory.

[28] H. A. Weidenmüller and G. E. Mitchell, Random matrices and chaos in nuclear physics: Nuclear structure, *Rev. Mod. Phys.* **81**, 539 (2009).

[29] C. W. Johnson, G. F. Bertsch, and D. J. Dean, Orderly spectra from random interactions, *Phys. Rev. Lett.* **80**, 2749 (1998).

[30] Y. M. Zhao, A. Arima, N. Shimizu, K. Ogawa, N. Yoshinaga, and O. Scholten, Patterns of the ground states in the presence of random interactions: Nucleon systems, *Phys. Rev. C* **70**, 054322 (2004).

[31] R. Bijker and A. Frank, Band structure from random interactions, *Phys. Rev. Lett.* **84**, 420 (2000).

[32] Y. Lei, Z. Y. Xu, Y. M. Zhao, S. Pittel, and A. Arima, Emergence of generalized seniority in low-lying states with random interactions, *Phys. Rev. C* **83**, 024302 (2011).

[33] Y. Lu, Y. M. Zhao, N. Yoshida, and A. Arima, Correlations between low-lying yrast states for sd bosons with random interactions, *Phys. Rev. C* **90**, 064313 (2014).

[34] J. J. Shen, H. Jiang, and G. J. Fu, Robustness of “noncollective” rotational behavior for nuclei in the presence of random interactions, *Phys. Rev. C* **104**, 054319 (2021).

[35] C. White, A. Volya, D. Mulhall, and V. Zelevinsky, Structured ground states of randomly interacting bosons, *Phys. Rev. Res.* **5**, 013109 (2023).

[36] G. J. Fu and C. Qi, Novel triaxiality-driven collective feature in atomic nuclei investigated via the two-body random ensemble, *Phys. Rev. C* **112**, L061301 (2025).

[37] G. J. Fu, J. J. Shen, Y. M. Zhao, and A. Arima, Regularities in low-lying states of atomic nuclei with random interactions, *Phys. Rev. C* **91**, 054319 (2015).

[38] Y. Lei, Y. M. Zhao, N. Yoshida, and A. Arima, Correlations of excited states for sd bosons in the presence of random interactions, *Phys. Rev. C* **83**, 044302 (2011).

[39] Y. Lei, Robust correlations between quadrupole moments of low-lying 2^+ states within random-interaction ensembles, *Phys. Rev. C* **93**, 024319 (2016).

[40] Z.-Z. Qin and Y. Lei, Predominance of linear q and μ systematics in random-interaction ensembles, *Nuclear Science and Techniques* **29**, 163 (2018).

[41] I. Stetcu and C. W. Johnson, Random phase approximation vs exact shell-model correlation energies, *Phys. Rev. C* **66**, 034301 (2002).

[42] I. Stetcu and C. W. Johnson, Tests of the random phase approximation for transition strengths, *Phys. Rev. C* **67**, 044315 (2003).

[43] I. Stetcu and C. W. Johnson, Gamow-teller transitions and deformation in the proton-neutron random phase approximation, *Phys. Rev. C* **69**, 024311 (2004).

[44] R. Lawson, *Theory of the Nuclear Shell Model*, Oxford studies in nuclear physics (Clarendon Press, 1980).

[45] M. Moshinsky, Transformation brackets for harmonic oscillator functions, *Nuclear Physics* **13**, 104 (1959).

[46] P. M. Larsen, K. W. Jacobsen, and J. Schiøtz, Rich ground-state chemical ordering in nanoparticles: Exact solution of a model for ag- au clusters, *Phys. Rev. Lett.* **120**, 256101 (2018).

[47] K. Jacobsen, P. Stoltze, and J. Norskov, A semi-empirical

effective medium theory for metals and alloys, *Surface Science* **366**, 394 (1996).

[48] G. Guisbiers, R. Mendoza-Cruz, L. Bazán-Díaz, J. J. Velázquez-Salazar, R. Mendoza-Perez, J. A. Robledo-Torres, J.-L. Rodriguez-Lopez, J. M. Montejan-Carrizales, R. L. Whetten, and M. José-Yacamán, *Electrum, the gold–silver alloy, from the bulk scale to the nanoscale: Synthesis, properties, and segregation rules*, *ACS Nano* **10**, 188 (2016).